Organic & Biomolecular Chemistry

ROYAL SOCIETY OF CHEMISTRY

PAPER

View Article Online
View Journal | View Issue

Check for updates

Cite this: *Org. Biomol. Chem.*, 2020, **18**, 495

Highly selective staining and quantification of intracellular lipid droplets with a compact push–pull fluorophore based on benzothiadiazole†

S. Israel Suarez,[a] Caroline C. Warner,[b] Heather Brown-Harding,[c] Andrea M. Thooft,[b] Brett VanVeller *[b] and John C. Lukesh, III *[a]

Received 18th November 2019,
Accepted 11th December 2019

DOI: 10.1039/c9ob02486g

rsc.li/obc

A robust lipophilic dye, based on the structures of the benzothiadiazole heterocycle, was shown to be a potent fluorescent stain for the selective imaging of lipid droplets (LDs) within both live and fixed human cells. Its small molecular framework, large Stokes shift, and vastly improved photostability over that of the current *status quo*, Nile Red, highlight its tremendous potential as a versatile chemical tool for facilitating LD imaging and research.

Introduction

Lipid droplets (LDs) are highly dynamic cellular organelles involved in the storage and metabolism of neutral lipids. The processing of LDs is tightly controlled, where mis-regulation is closely associated with various metabolic diseases such as obesity and cancer.[1–5] Thus, the selective detection and visualization of LDs is critical to the assessment of their relative abundance, size, distribution, and further elucidation of their fundamental roles in human health and disease. To this end, lipophilic dyes have proven to be invaluable chemical tools for advancing LD research by providing a non-destructive method for the imaging and quantification of LDs in real time—a necessary feature for probing LD dynamics within complex cellular environments.[6–14]

Of the reported LD stains, Nile Red (Fig. 1) is most commonly employed as a result of its commercial availability and long history as a reported LD marker.[15–17] However, the poor photostability and small Stokes shift of Nile Red results in high levels of noise and background artifacts.[18] Consequently, to better assess their primary and secondary roles under physiological conditions, there remains a need to develop new lipophilic fluorophores with enhanced photophysical properties and improved selectivity towards LDs.[19]

Chromophores based on the benzothiadiazole scaffold have received increasing attention in recent years for bioimaging applications.[20–22] Fluorophores that feature the benzothiadiazole core are often solvochromic and display comparatively large Stokes shifts. Benzothiadiazole derivatives also exhibit differences in emission intensity depending on the local solvent environment. In general, polar environments significantly quench fluorescence, whereas non-polar media 'turns-on' emission. These attributes have made benzothiadiazoles attractive for staining lipidic structures[23–25] and LDs in particular.[13,14]

The benzothiadiazole core can be decorated with targeting agents to help localize the fluorophore to the structure of inter-

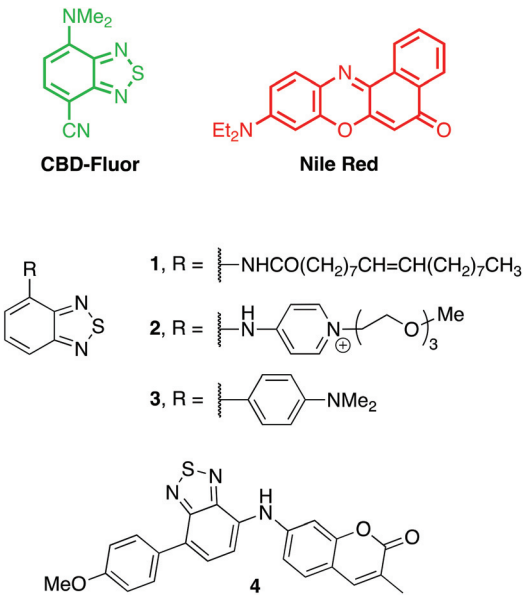

Fig. 1 Chemical structures of CBD-Fluor, Nile Red and other probes based on benzothiadiazole that have been used to image lipidic structures.

[a]*Department of Chemistry, Wake Forest University, Winston-Salem, NC 27101, USA. E-mail: lukeshjc@wfu.edu*
[b]*Department of Chemistry, Iowa State University, Ames, IA 50011, USA. E-mail: bvv@iastate.edu*
[c]*Department of Biology, Wake Forest University, Winston-Salem, NC 27101, USA*
†Electronic supplementary information (ESI) available. See DOI: 10.1039/c9ob02486g

est.[25] For example, the oleamide in **1** was proposed to assist in cellular uptake and the staining of LDs.[23] Similarly, the amphiphilic appendage in **2** was proposed to facilitate the targeting of lipid bilayers.[24] Notably, however, specific targeting agents are not necessary to image LDs, as evidenced by the prevalence of Nile Red as an LD marker. Indeed, both benzothiadiazole derivatives **3** and **4** have been reported to stain LDs within cells.[13,14] Presumably, this selectivity is due to the fluorescence turn-on behaviour of benzothiadiazoles within the hydrophobic core of lipid droplets. In this regard, the large hydrophobic surface area of **3**, **4** and even Nile Red leads to low solubility in water and an increase in non-specific staining of other hydrophobic structures that contribute to background. Herein, we report the use of a compact and more polar fluorophore, CBD-Fluor (Fig. 1),[26] that leads to more red-shifted wavelengths of emission, higher photostability, higher turn-on fluorescence response, and excellent contrast with background for the selective staining of lipid droplets.

Results and discussion

A critical element of design for benzothiadiazole chromophores that has been under utilized in the examples given in Fig. 1 is the application of a push–pull substitution pattern. The cooperative effects of appending an electron-releasing functional group (the push) in conjugation with an electron-withdrawing group (the pull) serves to dramatically red-shift the wavelengths of absorption and emission of chromophores. In the context of benzothiadiazoles, push–pull substitution patterns (such as the one exhibited by CBD-Fluor) can red-shift spectral features while maintaining a small size.[26,28–31]

Spectral characteristics of CBD-Fluor are ideal for LD imaging

The compact and polar structure of CBD-Fluor compared to other polycyclic aromatic dyes has the potential to improve solubility in water in order to diminish non-specific staining and disruption of native interactions. Despite this compact structure, however, CBD-Fluor emits similarly to larger cell-imaging dyes such as Nile Red, BODIPY, and fluorescein (>400 nm, Fig. 2A), but with a larger Stokes shift to limit signal from background. Moreover, CBD-Fluor displays marked photostability under continuous irradiation, in contrast to Nile Red, which rapidly photobleaches (Fig. 2B). Notably, CBD-Fluor is also more photostable than other benzothiadiazole dyes reported to stain LDs selectively.[14]

CBD-Fluor displays environmentally sensitive emission—high emission intensity in non-polar environments and diminished emission in polar environments (Fig. 3A). CBD-Fluor, however, displayed a stronger bias in this turn-on behavior relative to other LD-specific dyes (Fig. 3B),[13,14,23,26] with a limit of detection in dioxane that was less than 200 pM (Fig. S1†). Thus, we hypothesized that CBD-Fluor would be ideal for applications in lipid staining to address current shortcomings in standard LD analysis with Nile Red.

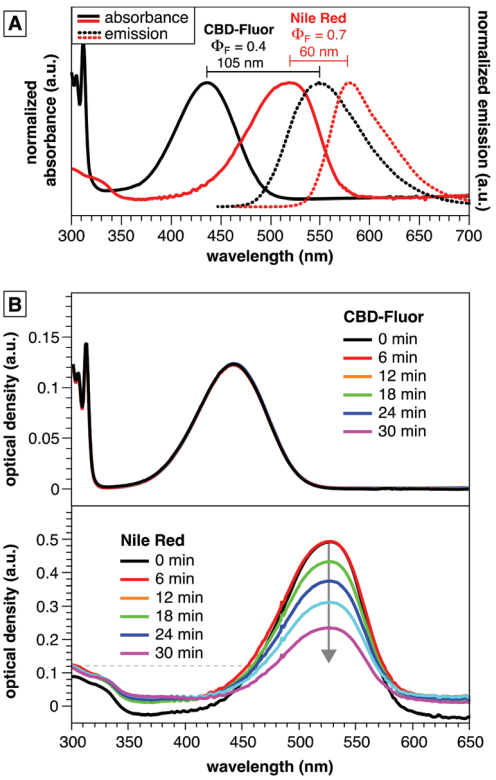

Fig. 2 (A) Emission spectra and quantum yield of CBD-Fluor and Nile Red in dioxane (B) photostability of CBD-Fluor[26] *versus* Nile Red[27] demonstrated by an unchanged absorption spectrum for CBD-Fluor *versus* photodecomposition of Nile Red. Solutions of each dye were prepared in air saturated THF with identical optical density (0.12 absorbance units) at 455 nm and were continuously irradiated using an LED source with an irradiance of 370 mW cm^{-2}.

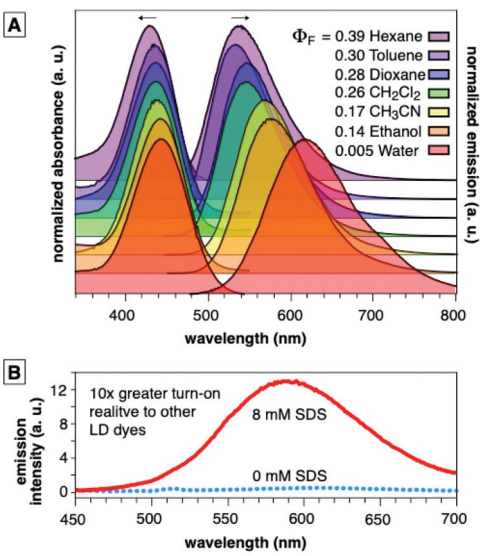

Fig. 3 (A) Absorbance and emission spectra for CBD-Fluor showing the solvent polarity and quantum yield effects in various solvents. See ESI† for details. (B) CBD-Fluor (10 μM) before and after addition of SDS (CMC = 8 mM). The turn-on in emission intensity of CBD-Fluor is larger than for previously reported benzothiadiazole dyes.[14,23]

Cellular imaging and microscopy

To initially assess the effectiveness of CBD-Fluor as an intracellular stain, both live and fixed HeLa (human cervical cancer) cells were incubated with CBD-Fluor and imaged using a confocal fluorescence microscope. The resulting images clearly depicted punctate staining, indicating that CBD-Fluor was indeed marking subcellular organelles (Fig. 4). To confirm that the spherical structures were lipid droplets, a separate experiment was performed in which live HeLa cells were co-incubated with both CBD-Fluor and Nile Red—the well-established LD stain.[15] Although both dyes were excited at 488 nm, given their distinct emission profiles, we were able to use linear unmixing (see ESI† for details) to assign a stained structure to either CBD-Fluor, Nile Red, or both (Fig. 4). Manders's co-localization coefficient (MCC) was then used to determine the co-occurrence of each dye.[32] We found that for spherical structures stained by CBD-Fluor, Nile Red would also be present 98% of the time, thus not only confirming co-localization of the two dyes but unequivocally establishing that the stained spherical structures were indeed lipid droplets. A positive correlation between CBD-Fluor and Nile Red was further established by determining Pearson's correlation coefficient (PCC) which was found to be 0.5. Although this value indicates a relatively strong correlation between the two dyes, it is likely reduced by the low signal-to-background of Nile Red.

To ensure that CBD-Fluor and Nile Red were staining spherical structures within the cell and not on the cell's surface, an orthogonal analysis was performed (see ESI†). A total of 11 slices at 10 μm were analyzed along the *Z*-axis. This analysis established that CBD-Fluor was staining spherical structures within the cell. Co-localization studies with Nile Red further confirmed that these spherical structures were in fact lipid droplets.

Given their complex structural makeup, one of the few reliable methods for identifying all intracellular LDs is by staining their hydrophobic core with a lipophilic dye. Therefore, to better evaluate CBD-Fluor's LD staining capabilities, we set out to evaluate how easily we could quantify the total number of lipid droplets within both fixed and live cells using CBD-Fluor as a selective fluorescent marker. Given the performance features of CBD-Fluor: (i) improved water solubility—especially compared to other lipophilic dyes (*i.e.* Nile Red), (ii) impressive photostability, and (iii) remarkable turn-on response within a lipophilic environment, we reasoned that these attributes would reduce background artifacts and provide an enhanced signal-to-noise ratio (S/N). Critically, better S/N performance facilitates the use of standard automated image analysis techniques to quantify intracellular lipids (see ESI†). Using this technique in live HeLa cells, we were able to stain an average of over 11 LDs per cell with CBD-Fluor (Fig. 5A and B). Moreover, similar results were obtained within fixed HeLa cells as an average of nearly 16 LDs per cell were clearly marked with CBD-Fluor (Fig. 5C and D).

To better visualize the extraordinary turn-on response of CBD-Fluor, a 2D histogram was generated that depicts the relative fluorescence intensity of CBD-Fluor across the entire diameter of a cell (Fig. 6A). Indeed, CBD-Fluor displayed stark turn-on response with a greater than 300-fold increase in relative fluorescence intensity when trapped within the hydrophobic core of a cellular LD. Conversely, with Nile Red (Fig. 6B), a less than 30-fold increase in turn-on fluorescence was observed relative to background. These results further demonstrate CBD-Fluor's potential as a reliable and more selective LD marker within a complex cellular environment.

Finally, and to further demonstrate the overall utility of CBD-Fluor as an intracellular stain, we also showed that it could be used to effectively visualize LDs in the presence of other cellular dyes. Upon co-incubation of CBD-Fluor (green emission) and Hoechst, a common nuclear stain (blue emission), the resulting images were obtained (Fig. 7). Overlay of these signals validated the ease with which CBD-Fluor can be used to image LDs alongside other cellular markers allowing one to track different subcellular organelles simultaneously.

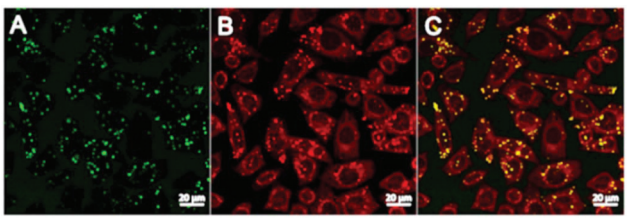

Fig. 4 Live HeLa (human cervical cancer) cells stained for lipid droplets with (A) CBD-Fluor (ex: 488 nm, em: 539 nm), (B) Nile Red (ex: 488 nm, em: 565 nm), and (C) overlay of images. Scale bar is set to 20 μm. Mander's co-localization coefficient (MCC) = 0.98. Pearson's correlation coefficient (PCC) = 0.50.

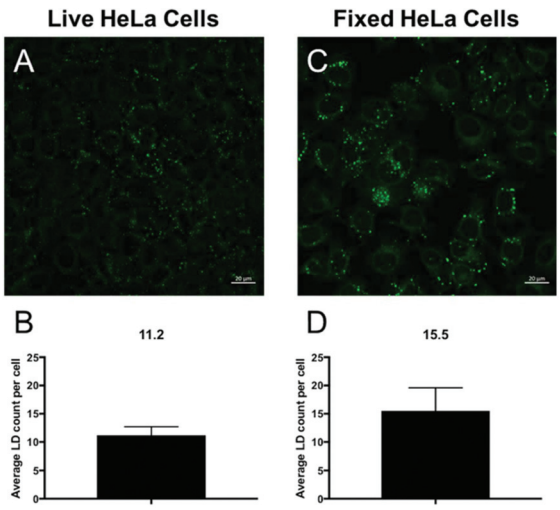

Fig. 5 The average LD count per cell with CBD-Fluor in both live (A and B) and fixed (C and D) HeLa cells. The reported values are the average ± STD over three distinct sampling images. Scale bar is set to 20 μm.

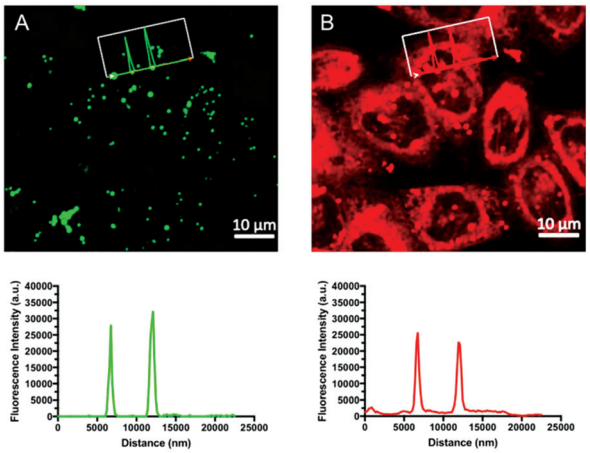

Fig. 6 Representative 2D-histograms of CBD-Fluor (A) and Nile Red (B) that display the relative fluorescence intensity of each dye across the entire diameter of a cell. On average CBD-Fluor displayed a greater than 10-fold improvement in signal-to-noise relative to that of Nile Red. MCC = 0.98 and PCC = 0.50. Scale bar is set to 10 μm.

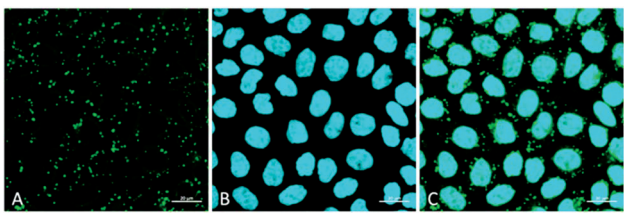

Fig. 7 Cellular staining with (A) CBD-Fluor (ex: 488 nm, em: 539 nm and (B) Hoechst (ex: 405 nm, em: 453 nm). (C) Overlay of respective images. Scale bar is set to 20 μm.

Conclusions

CBD-Fluor, a robust and versatile push–pull fluorophore was shown to be a highly effective stain for the imaging and quantification of LDs within both fixed and live human cells. Given its impressive S/N, high biocompatibility, and vastly improved photostability over that of Nile Red, render CBD-Fluor a highly attractive chemical reporter for facilitating both LD imaging and research.

Conflicts of interest

There are no conflicts to declare.

Acknowledgements

JCL is thankful for financial support from Wake Forest University (Start-up funds). BV is grateful for support of this work by the National Science Foundation under Grant No. 1848261.

Notes and references

1 Y. Guo, K. R. Cordes, R. V. Farese and T. C. Walther, *J. Cell Sci.*, 2009, **122**, 749–752.
2 B. Brügger, *Annu. Rev. Biochem.*, 2014, **83**, 79–98.
3 P. Shyu, X. F. A. Wong, K. Crasta and G. Thibault, *Biosci. Rep.*, 2018, **38**, BSR20180764.
4 M. H. den Brok, T. K. Raaijmakers, E. Collado-Camps and G. J. Adema, *Trends Immunol.*, 2018, **39**, 380–392.
5 J. A. Olzmann and P. Carvalho, *Nat. Rev. Mol. Cell Biol.*, 2019, **20**, 137–155.
6 L. D. Lavis and R. T. Raines, *ACS Chem. Biol.*, 2008, **3**, 142–155.
7 A. B. Neef and C. Schultz, *Angew. Chem., Int. Ed.*, 2009, **48**, 1498–1500.
8 J. Spandl, D. J. White, J. Peychl and C. Thiele, *Traffic*, 2009, **10**, 1579–1584.
9 J. Chan, S. C. Dodani and C. J. Chang, *Nat. Chem.*, 2012, **4**, 973–984.
10 E. Kim, S. Lee and S. B. Park, *Chem. Commun.*, 2012, **48**, 2331.
11 H.-J. Yang, C.-L. Hsu, J.-Y. Yang and W. Y. Yang, *PLoS One*, 2012, **7**, e32693.
12 A. Goel, A. Sharma, M. Kathuria, A. Bhattacharjee, A. Verma, P. R. Mishra, A. Nazir and K. Mitra, *Org. Lett.*, 2014, **16**, 756–759.
13 H. Appelqvist, K. Stranius, K. Börjesson, K. Peter, R. Nilsson and C. Dyrager, *Bioconjugate Chem.*, 2017, **28**, 1363–1370.
14 A. A. R. Mota, J. R. Correa, L. P. de Andrade, J. A. F. Assumpção, G. A. de Souza Cintra, L. H. Freitas-Junior, W. A. da Silva, H. C. B. de Oliveira and B. A. D. Neto, *ACS Omega*, 2018, **3**, 3874–3881.
15 P. Greenspan, *J. Cell Biol.*, 1985, **100**, 965–973.
16 I. A. Boldyrev, X. Zhai, M. M. Momsen, H. L. Brockman, R. E. Brown and J. G. Molotkovsky, *J. Lipid Res.*, 2007, **48**, 1518–1532.
17 J. Rumin, H. Bonnefond, B. Saint-Jean, C. Rouxel, A. Sciandra, O. Bernard, J.-P. Cadoret and G. Bougaran, *Biotechnol. Biofuels*, 2015, **8**, 42.
18 T. Govender, L. Ramanna, I. Rawat and F. Bux, *Bioresour. Technol.*, 2012, **114**, 507–511.
19 T. Fam, A. Klymchenko and M. Collot, *Materials*, 2018, **11**, 1768.
20 A. S. Klymchenko, *Acc. Chem. Res.*, 2017, **50**, 366–375.
21 B. A. D. Neto, P. H. P. R. Carvalho and J. R. Correa, *Acc. Chem. Res.*, 2015, **48**, 1560–1569.
22 A. P. Demchenko, G. Duportail, S. Oncul, A. S. Klymchenko and Y. Mély, in *Methods in Membrane Lipids*, ed. D. M. Owen, Springer New York, New York, NY, 2015, vol. 1232, pp. 19–43.
23 A. A. R. Mota, P. H. P. R. Carvalho, B. C. Guido, H. C. B. de Oliveira, T. A. Soares, J. R. Corrêa and B. A. D. Neto, *Chem. Sci.*, 2014, **5**, 3995.
24 P. H. P. R. Carvalho, J. R. Correa, K. L. R. Paiva, D. F. S. Machado, J. D. Scholten and B. A. D. Neto, *Beilstein J. Org. Chem.*, 2019, **15**, 2644–2654.
25 A. S. Klymchenko and R. Kreder, *Chem. Biol.*, 2014, **21**, 97–113.

26 A. M. Thooft, K. Cassaidy and B. VanVeller, *J. Org. Chem.*, 2017, **82**, 8842–8847.
27 D. L. Sackett and J. Wolff, *Anal. Biochem.*, 1987, **167**, 228–234.
28 S. R. Norris, C. C. Warner, B. J. Lampkin, P. Bouc and B. VanVeller, *Org. Lett.*, 2019, **21**, 3817–3821.
29 S. Uchiyama, T. Santa, T. Fukushima, H. Homma and K. Imai, *J. Chem. Soc., Perkin Trans. 2*, 1998, 2165–2174.
30 S. Uchiyama, K. Takehira, S. Kohtani, K. Imai, R. Nakagaki, S. Tobita and T. Santa, *Org. Biomol. Chem.*, 2003, **1**, 1067–1072.
31 S. Uchiyama, K. Kimura, C. Gota, K. Okabe, K. Kawamoto, N. Inada, T. Yoshihara and S. Tobita, *Chem. – Eur. J.*, 2012, **18**, 9552–9563.
32 K. W. Dunn, M. M. Kamocka and J. H. McDonald, *Am. J. Physiol.: Cell Physiol.*, 2011, **300**, C723–C742.